The Cryosphere
Open Access
Discussions

The influence of surface characteristics, topography, and continentality on mountain permafrost in British Columbia

A. Hasler[1,2], M. Geertsema[1], V. Foord[1], S. Gruber[3], and J. Noetzli[4]

[1]Ministry of Forest, Land and Natural Resources Operation of British Columbia, 1044 Fifth Avenue, Prince George BC V2L 5G4, Canada
[2]Department of Geosciences, University of Fribourg, Chemin du Musee 4, 1700 Fribourg, Switzerland
[3]Department of Geography and Environmental Studies, Carleton University, 1125 Colonel By Drive, Ottawa ON K1S 5B6, Canada
[4]Glaciology, Geomorphodynamics and Geochronology, Department of Geography, University of Zurich, Winterthurerstr 190, 8057 Zurich, Switzerland

TCD

8, 4779–4822, 2014

Characteristics of mountain permafrost in British Columbia

A. Hasler et al.

Title Page

Abstract	Introduction
Conclusions	References
Tables	Figures

|◄ | ►|

◄ | ►

Back | Close

Full Screen / Esc

Printer-friendly Version

Interactive Discussion

Abstract

Thermal offset and surface offset are terms that describe the deviation of the mean annual ground temperature from the mean annual air temperature. These offsets are controlled by surface characteristics and topo-climatic factors on a micro- and meso-scales. Macro-climatic conditions may, however, influence the effectiveness of the responsible processes. Existing knowledge on surface- and topography-specific offsets is not easily transferable and limits the applicability of empirical permafrost distribution models over large areas with macro-climatic gradients. In this paper we describe surface and thermal offsets derived from distributed measurements at seven field sites in British Columbia. Key findings are (i) a surprisingly small variation of the surface offsets between different surface types and small thermal offsets in general (excluding wetlands and peat), (ii) a clear influence of the micro-topography at wind exposed sites (snow cover erosion), (iii) a north–south difference of the surface offset of 4 °C in near-vertical bedrock and of 1.5–3 °C on open (no canopy) gentle slopes, (iv) only small macro-climatic differences caused by the reverse influence of snow cover thickness and annual air temperature amplitude. These findings suggest, that empirical permafrost models based on topo-climatic variables may be applicable across regions with significant macro-climatic differences.

1 Introduction

To estimate permafrost distribution and characteristics knowledge of site specific coupling between the lower atmosphere and ground is needed. Surface offsets (SO), defined as MAGST minus MAAT (where MAGST is the mean annual ground–surface temperature and MAAT is the mean annual air temperature), and thermal offsets (TO), defined as TTOP minus MAGST (where TTOP is the mean annual temperature at the top of permafrost), are terms to describe this coupling (Lunardini, 1978). These offsets depend on local climatic and topographic conditions as well as the surface charac-

Characteristics of mountain permafrost in British Columbia

A. Hasler et al.

teristics because these conditions cause a large variability in (solar and long-wave) radiation, snow cover insulation and near-surface heat transfer. Empirical permafrost models implicitly apply the concept of these offsets by estimating the ground thermal conditions (or permafrost probability) based on MAAT (or elevation) and proxy-variables of the topo-climatic effects and the surface conditions (Riseborough et al., 2008). The assessment of the variation and control of surface and thermal offsets in the mountain ranges of British Columbia, Canada, is therefore essential for an estimation of the province wide permafrost distribution and the analysis of related natural hazard. This study presents the first distributed ground temperature records in potential permafrost areas of this region, which are necessary for such a task.

For mountain permafrost the influence of (steep) topography is well described for some mid-latitude mountain ranges considering meso-scale variability in solar radiation (insolation), air temperature, snow deposition and snow redistribution (cf. Harris et al., 2009 for a literature review on this subject). The influence of surface characteristics on mountain permafrost is addressed in some case studies (Gubler et al., 2011; Schneider et al., 2012) for high-alpine surface types. British Columbia's higher latitude with mountain permafrost extending below tree line, however, alters the influence of the surface characteristics and topography compared to the permafrost in the Alps or other mid-latitude mountain ranges. Studies elsewhere in Canada (Harris, 2008; Bonnaventure et al., 2012) are either not spatially distributed or rely on BTS measurements so they can not be easily extrapolated (without local permafrost evidences) to our study region. Hence, we aim to estimate the region-specific variation of the temperature offsets (SO, TO) dependent at micro- and meso-scale gradients in surface characteristics and topography.

At the macro-climatic scale, variations in MAAT are the primary determinant of permafrost occurrence (Throop et al., 2012). While MAAT variations are relatively easily captured in flat terrain with interpolation products or climate re-analysis datasets, mountain topography adds large uncertainties to such estimates due to variations in the air temperature lapse rate (Fiddes and Gruber, 2014). Further, an important issue

to estimate the permafrost conditions on the large-scale is the question if the surface offset (SO) is strongly influenced by macro-climatic parameters (e.g. precipitation and continentality). This question is an other focus of this study because British Columbia and our field sites span a large gradient in macro-climatic conditions.

Due to the patchy characteristics of our data, this paper comprises a detailed description of the data processing and resulting uncertainties in SO and TO (Sect. 3.1 and 3.2). Accordingly, one scope of the paper is to provide a method to threat data gaps, which are typical for distributed GST (ground–surface temperature) records. For illustration purpose in the discussion (Sect. 4) we briefly introduce a 3-dimensional heat conduction model (Sect. 3.3) and a simple thermal diode model (Sect. 3.4). In Sect. 4.1 we present the field data and discuss them (and respective model results) regarding the three mentioned gradients (Sect. 4.2 surface characteristics; 4.3 topography and 4.4 macro-climate): these 3 gradients are important for the mountain permafrost distribution and the interpretation of its prediction (permafrost maps) in British Columbia.

2 Field sites and instrumentation

2.1 General site description

The macro-topography of British Columbia is characterized by two major mountain systems, the Coast Mountains and the Rocky Mountains, with plateaus and lesser ranges between them (Fig. 1). Being at mid latitude (49–60° N), within the west-drift zone, the general meridional orientation (NNW to SSE) of these mountain systems is responsible for pronounced differences in climatic conditions between their coastal and continental sides. Large gradients in precipitation and continentality (annual temperature amplitude for a given latitude) characterize the climate of British Columbia (Fig. 1). These differences exist both at a macro-climatic scale with continentality increasing with distance from the Pacific Ocean, and also at a meso-scale with orographic effects such as pronounced temperature inversions in the interior valleys. Hence, an extreme west–east

gradient exists in the Coast Mountains and continentality is particularly pronounced at lower elevations in, and east of, the Rocky Mountains (Wang et al., 2012).

The seven field sites of this study are located in northern BC between 54°45′ and 59° N. One is in the Coast Mountains (HUD: Hudson Bay Mtn.), two are in the Rocky Mountains (NON: Nonda, POP: Poplars) and four are at the occidental edge of the Rocky Mountains (GUN: Mt. Gunnel, TET: Tetsa, PIN: Pink Mountain, MID: Middlefork) (Fig. 1). HUD, NON, GUN and PIN are high elevation sites, which means they are above the tree line and at or near mountain tops while the other sites are below tree line and close to the valley floor, or in relatively flat areas. The climate at the field sites, ranges from moderate-humid alpine (Coast Mts.) to subarctic-continental (lowland north-eastern BC). The mean annual air temperature (MAAT) at all sites is in the range of −5 to +1 °C (Wang et al., 2012), hence at all sites both permafrost and non-permafrost conditions are plausible depending on their local characteristics. In even warmer conditions, permafrost only occurs in very unusual circumstances such as rock glacier lobes or avalanche/debris cones.

The Nonda (1670 m a.s.l.), Pink Mountain (1750 m a.s.l.), and Hudson Bay Mountain sites (∼ 1950–2150 m a.s.l.) are clearly within the Alpine Tundra (AT) biogeo-climatic zone (Meidinger and Pojar, 1991) above treeline. The Mount Gunnel sites (1470 m a.s.l.) are at the lower boundary of the AT zone, above treeline, but transitioning into the forested Black and White Boreal Spruce (BWBS) zone. With the exception of Hudson Bay Mountain, all of these alpine sites are strongly windswept, resulting in very little snow cover.

The remaining sites occur well within forested biogeoclimatic zones. The Middlefork cluster (1000 m) is well within the BWBS zone, but includes a permafrost-underlain peat plateau (dominated by *Sphagnum* and a sparse cover of black spruce (*Picea mariana*)), a treeless cold air drainage meadow, and a zonal forest of white spruce (*Picea glauca*) and aspen (*Populus tremuloides*). The Poplars (750–940 m a.s.l.) and Tetsa (1000 m a.s.l.) sites are forested and fall within the Spruce Willow Birch (SWB) zone. Both are instrumented along elevation gradients on north and south facing ex-

posures. There is striking aspect control on vegetation here. South-facing slopes host trembling aspen (*Populus tremuloides*) and lodgepole pine (*Pinus contorta*) and may have a grassy understory. Forest floors have relatively thin humus forms. North-facing slopes tend to have a sparse cover of black spruce (*Picea mariana*) and very thick mor (mossy) humus forms. Permafrost can usually be found some 60 cm below the forest floor.

Using instrumental data from nearby Environment Canada weather stations, climate trends (1912–2003) for the region containing the Hudson Bay Mountain field site have increased significantly by 0.8 °C in mean annual temperature (Egginton, 2005). Climate trends (1937–2003) for the region containing the remaining field sites in north-east BC have a significant increase of 1.3 °C in mean annual temperature, 3.3 °C significant increase in extreme minimum temperature, and a 42 % significant decrease in winter precipitation (Egginton, 2005).

2.2 Measurement parameters and instrumentation

The seven field sites vary regarding the sampling the local conditions (topographic situation and surface characteristics) and so does the measurement setup. This non-standardised and not strictly systematic design is on one side due to absence/presence of various local conditions between field sites: e.g. steep bedrock is present only at some high-elevation sites whereas surface characteristics such as thick moss layers or forests are not covered there (Table 1). On the other hand, some parameters are challenging to obtain or meaningless at local scale (e.g. air temperature in rock faces or direct radiation in forests). The distance between individual measurement locations ranges from some decametres (e.g. GUN and NON site) to a few kilometers (low elevation sites POP, TET, and MID). For these reasons meteorological parameters are measured at one central location (wx) per high elevation site. The low elevation sites have air temperature measurements at each location similar to the setup of comparable studies in north-western Canada (Karunaratne and Burn, 2003).

Characteristics of mountain permafrost in British Columbia

A. Hasler et al.

Title Page

Abstract	Introduction
Conclusions	References
Tables	Figures

|◄   ►|

◄   ►

Back   Close

Full Screen / Esc

Printer-friendly Version

Interactive Discussion

The measured parameters are the temperature of the air (T_{air}), the ground–surface (T_{surf}), and the ground (T_{ground}). The ground temperatures are sensed at a depth between 0.3 and 1.3 m for soils and debris, but at 0.1 m depth for bedrock. At the central weather stations (wx) other parameters such as rainfall, relative humidity, direct short wave irradiation, wind direction and speed, and barometric pressure are measured but used only as Supplement in the present analysis. The weather stations are Onset Hobo Weather Station (H-21 or U30) and air temperature is measured in a solar radiation shield at 1.4 m above ground with a *S-THB-M002 Temperature/RH Smart Sensor (Tempcon),* which provides an accuracy of ±0.2 °C above 0 °C and ±0.4 °C above –30 °C. The other temperatures are recorded with *Hobo U23 pro V2* 2-channel mini loggers (*Onset*) which provide a similar accuracy. For air temperature the external sensors of the mini loggers are shielded with a similar radiation shield at 1.4 m height. Ground surface temperature is usually recorded with the internal temperature sensor of the mini logger, which is buried a few centimeters in the organic layer or debris, to minimize albedo effects. For near-surface rock temperatures an external sensor is placed in a small drilling and sealed with silicon glue. Physical disturbances (e.g. radiation influence of air temperature) are assumed to be below the sensor accuracy (cf. Nakamura and Mahrt, 2005) on the level of daily aggregates and even smaller for annual mean. Temperatures are sensed at 4 min sample intervals and aggregated and stored to hourly values.

The field sites selected and the sampling of local conditions, reflect the focus on mountain permafrost. Gradients in hydrological conditions (wetlands, peats etc.) are barely considered in this study despite their important role for the permafrost distribution in low-land areas. Table 1 summarizes the topographic situations and surface characteristics of the 41 locations with ground temperature measurements and the three weather stations analysed in this study. In the discussion section (4.2) we will refer to these local conditions in more detail.

3   Data processing and analysis methods

3.1   Pre-processing of raw temperature time series

At the field sites MID, NON and POP measurements were initiated in summer 2007, whereas, data acquisition started in 2008 for the other field sites. The data time series for this analysis were retrieved between summer 2011 and 2013 for the last time. Figure 2 gives an overview of the data completeness after filtering of invalid data. This filtering comprises two procedures and produces gaps of different characteristics: (a) automated filtering of invalid/corrupted values (not numeric or out of realistic range) cause short gaps (gap type I: single values), (b) manual filtering of values from broken sensors (e.g. water damage or cable disruption) are applied over long time periods and cause long gaps (gap type II: weeks to months). Maintenance effects on logger operation lead to missing data with the following characteristics: data read out lead to type I gaps while low power supply lead to type II gaps. The majority of the gaps observed in our data is of type II mainly caused by sensor damage and low battery except for the air temperature on Pink Mt. (Fig. 2). Because of these gaps it is not possible to directly compare all time series and simply calculate annual means for the same years. To account for this data characteristic we applied the processing described in Sect. 3.2.

For all the data analysed in this study there is at least one continuous year of valid data. One exception is the air temperature measurement of the weather station at Mt. Gunnel. The very good correlation of 11 months existing data with the surface temperature recorded in a near-by rock cleft allow a reliable estimation of the mean annual air temperatures. The related data and linear regression model (LRM) is presented in Fig. 3. The standard error for a 365 days mean is 0.015 °C (residual std. error/sqrt(n) with $n = 24 \times 365$).

3.2 Calculation of mean annual temperatures and their inter-comparability

Annual means of temperature time series (MAT) depend on the averaging period and the completeness of the raw data (Fig. 3). Surface and thermal offsets, the differences between such annual means, are highly error sensitive to this mean calculation. As described above, our data is characterized by inconsistencies regarding the available measurement periods and data completeness. To minimize errors introduced by the data aggregation and to avoid misinterpretations of the resulting offsets due to temporal variations, we conduct the following processing steps: 1. Calculate daily mean temperature; 2. Calculate running mean annual temperature; 3. MAT statistics; and 4. Surface and thermal offsets calculation.

The hourly data is aggregated to daily means. Gaps up to two missing values per day are interpolated, if more values are missing no value ("NA") is introduced to the daily mean data. This is important to avoid effects of systematic type I gaps.

Then, running mean annual temperatures (RMAT) are calculated for a 365 day window with 99 % of data available (Fig. 4). In Fig. 4 the example of Pink Mt. illustrates possible problems with the inter-comparability of annual means if time series are incomplete or if the running means are asynchronous: MATs from different points in time cannot be easily compared and offsets between RMATs vary strongly for some locations (Fig. 4b). This is considered with the next two steps of the data processing, the MAT statistics calculation and the surface/thermal offset calculation.

For the MAT statistics the mean and the spread of all RMAT values are calculated (minima, maxima and standard deviation) over the entire available data. This allows us to obtain a MAT value independent of sufficient data within particular calendar years and to get measures for the temporal variation of the MATs. We use the min.- and max.-values as indicator of MAT spread (Fig. 4b), because the variations are not normally distributed. For short RMAT time series (below 50 % of longest time series at field site), the means and spreads are corrected by using a longer time series as a reference. As a reference the RMAT time series from the same field site with the best correlation dur-

ing the overlapping time period is chosen (e.g. cx_Tsurf for wx_Tair at Pink Mt., Fig. 4). The mean annual temperature of such a short temperature time series is estimated by:

$$MAT = \overline{RMAT_{overlap}} - \overline{RMAT_{ref\_overlap}} + \overline{RMAT_{ref}} \tag{1}$$

with $RMAT_{overlap}$ being the RMAT time series of interest where it overlaps with the reference, $RMAT_{ref\_overlap}$ being the reference time series of the same period and $RMAT_{ref}$ being the mean of the entire reference time series. The uncertainties of this estimate are approximated by

$$U_{MAT} = \sigma(RMAT_{overlap} - RMAT_{ref\_overlap}) \times \frac{\sigma(RMAT_{ref})}{\sigma(RMAT_{ref\_overlap})} \tag{2}$$

assuming that the variations of the difference of the two variables scales with the relative variance captured by the overlapping period. This uncertainty is then added/subtracted to max./min. values of the MAT statistics of the temperature of interest, resulting in a larger spread for shorter time series (higher uncertainty; cf. Fig. 4b PIN_wx_Tair). The uncertainty introduced by measurement errors and data pre-processing (about $\pm 0.2\,°C$) are small compared to the temporal variations and negligible for the MAT statistics if considered as independent errors (root of square sum). Figure 5 shows the result of the MAT statistics on the example of Pink Mountain, which is a worst case in terms of data continuity: *W_Trock* or the *ls_Tsurf* MAT values show spreads up to $4.5\,°C$ due to the limitation of the available data.

The surface and thermal offsets are calculated by a simple subtraction of the MAT values. However, the spread of these offsets is smaller than spreads of the MATs in many cases because the temporal variations of RMATs are often synchronous (cf. Fig. 4a). Given this, the minimum and maximum difference between the RMATs (e.g. $SO_{min/max}$ at GUN_W) is used as indication of the uncertainty of the offsets, introduced by temporal variation of the SO (Fig. 4a). Where only short time series (less than 50 % of longest time series) or no overlap between RMATs exists, the spreads of the MAT

statistics are added to obtain a conservative (large) uncertainty estimate (cf. $SO_{min/max}$ of PIN_SE in Fig. 4b). To these uncertainty values an independent measurement error of ±0.3 °C is added (square root of quadratic sum) to obtain a total uncertainty for each temperature offset (c.f. Hasler et al., 2011).

$$U_{offset} = \sqrt{(Offset_{max} - Offset_{min})^2 + 0.6^2} \tag{3}$$

For the Hudson Bay Mt. field site, where the air temperature is measured at a meteorological station at 300 m to 500 m lower elevation (Table 1), an air temperature lapse rate between −3.75 to −6.25 °C km^{-1} is used for the calculation of the mean annual air temperature (MAAT), the SO and its uncertainty. In Fig. 5b an example of a temperature profile shows the surface and thermal offset at one location at Pink Mt. In the further analysis, offsets are treated as significant (solid lines) if they are larger than the (inner) half of the uncertainties ($U_{offset}/2$) indicated by the spreads in Fig. 5b.

The annual temperature amplitudes (ATA) used in this article are the differences between mean July and January temperatures divided by 2. The N factors used in the discussion of the snow cover influence are calculated on a seasonal and biweekly basis by dividing the mean surface temperature (or freezing index If) through the mean air temperature (T_{surf}/T_{air} or If_{surf}/If_{air}). Because the relative errors of these calculations are much smaller, we do not detail these calculations and their uncertainties here.

3.3 Heat conduction model for visualisation of rock temperatures

For the visualization of the aspect-dependent rock surface temperatures and the cooling effect of air-ventilated clefts on the subsurface thermal field we apply a three-dimensional heat conduction model of the Gunnel field site. The simulation is based on the approach by Noetzli (2008), to which we refer for details on the modeling procedure, sensitivity studies, and validation.

The geometry of the Gunnel blocks was created based on the footprint of aerial photos available in Google Earth with an estimated height of 10–30 m. Two overlapping cones and a rectangular box of 100 m height were added below. The geometry

was meshed with increasing element size from the surface to the interior. The upper boundary conditions (UBC, Dirichlet) were derived from the typical mean annual ground surface temperature (MAGST) of the data described above: the flat surfaces on top of the blocks were set to $-0.65\,°C$ and all cleft surfaces to $-1.5\,°C$. For the near-vertical side walls a function $T_{surf} = f(\text{aspect})$ was obtained by fitting a sine curve through the MAGST of the six steep measurement locations to interpolate values for the aspect of the rock faces with no measurements. A significant effect of a bottom heat flow is not expected for the Gunnel blocks and the lower boundary condition is set to thermal insulation. The subsurface temperature field was calculated based on three-dimensional conductive heat transport within the modelling package COMSOL Multiphysics (Software by Femlab AG). Subsurface properties were assumed to be isotropic and homogeneous for the entire cross section and set to typical values for sandstone: specific heat capacity $900\,J\,kg^{-1}\,K^{-1}$, density $2300\,kg\,m^{-3}$ and thermal conductivity $2.3\,W\,K^{-1}\,m^{-1}$ (Cermak and Rybach, 1982). Latent heat was considered based on an apparent heat capacity approach as described by Mottaghy and Rath (2006), saturated conditions and a bulk porosity of 5 % (gritstone). Effects from past climate variations are assumed to be negligible for the small size of the Gunnel blocks (Noetzli and Gruber, 2009). To describe the development of an active layer, a transient model run was performed. For this, the surface temperature evolution during the course of the year is prescribed, based on the average of the monthly means of all loggers. After a spin-up period of 4 years, the simulation was eventually performed for one year free time steps of maximum 7 days. For comparison, simulations were performed with and without clefts in the blocks as well as in- and excluding the effect of latent heat.

3.4 The thermal diode model for snow-cover effects

A reductionist model is applied to illustrate the reverse influence of two macro-climatic variables, annual temperature amplitude and precipitation (or snow cover thickness). The thermal diode effect in frozen soils refers to temperature dependent heat transfer and results in offsets in mean annual temperatures. The presence/absence of the snow

Characteristics of mountain permafrost in British Columbia

A. Hasler et al.

cover acts similarly as such a thermal diode between atmosphere and ground surface. The term thermal diode is borrowed from the electrical semi-conductor element. The electro-technical scheme in Fig. 6 is a representation of this situation.

A numerical implementation in R (statistical programming language) of this simple scheme is used to simulate the relative effect of different snow cover insulation (R_s) and annual amplitudes of T_{air} being inversely proportional to each other. For a given T_{air} the ground surface temperature T_{surf} is calculated by a division according to the (heat) resistances (voltage divider equation):

$$T_{surf} = T_{ground} + (T_{air} - T_{ground})\frac{R_{gr}}{R_{gr} + R_s} \mid T_{air} < T_{ground}$$

$$T_{surf} = T_{ground} + (T_{air} - T_{ground})\frac{R_{gr}}{R_{gr}} = T_{air} \mid T_{air} \geq T_{ground} \qquad (4)$$

The model is initialized with the MAT for T_{surf} and T_{ground}. For Eq. (1), T_{ground} is taken from the previous time step [$i-1$] (because $dT_{ground}/dt \ll dT_{air}/dt$) and the new ground temperature is calculated as follows:

$$T_{ground}[i] = T_{ground}[i-1] + \frac{mean(T_{surf}[i-1, i]) - T_{ground}[i-1]}{R_{gr} \cdot C_{gr}} \qquad (5)$$

Different versions of this thermal diode model are compared in a brief sensitivity analysis. These models are small modifications of the scheme above to which we refer as exact model. For the n factor model (n factor after (Lunardini, 1978): Nfreez/Nthaw = $1/(1 + Rs)$ which is the model above with $R_{gr} = 1$) snow cover insulation is triggered if $T_{air} < 0\,°C$ (instead of $T_{air} < T_{ground}$); temperature dependent snow cover insulation ($R_s = f(T_{air})$) and a time lag between T_{air} and snow cover build-up is applied in the variable insulation model; additionally latent heat effects where simulated with $T_{surf} = 0\,°C$ if $T_{air} > 0\,°C$ and snow cover present as a subversion of the variable insulation model.

Full Screen / Esc

Printer-friendly Version

Interactive Discussion

Some examples of this sensitivity analysis are given together with the discussion of the modelling results. The absolute values of the SOs vary between model types up to 50 % but the ratio between simulated SOs in a prototypic continental and maritime climate remains very similar for all model versions. Given the purpose of qualitative illustration, this simple model provides sufficiently robust results.

4 Results and discussion

4.1 Overview of the mean annual temperatures and offsets

Figure 7 gives an overview of all MAT profiles and the significance of the surface and thermal offsets. Trends in MAAT are in the order of 0.1–0.2 °C decade^{-1} (cf. Sect. 2). Hence, in the near surface temperatures that are considered in these profiles we do not expect mid-term transient effects by air temperature changes unless the ground is isothermal at 0 °C with a high ground ice content. However, trends in snow cover evolution during the last two decades are difficult to estimate for the individual locations and may lead to an enhanced uncertainty for profiles with a strong dependency on snow cover (e.g. in convex topography). This lower correlation with air temperature is reflected by the calculation of the offset uncertainty (Sect. 3.2) and leads to insignificant surface offsets (SOs) even if the absolute values of the offsets are large (dashed lines in Fig. 7; e.g. at locations *PIN_cc* or *TET_S1/S2*).

All sites show MAATs below zero degrees Celsius except *Poplars-S,* which has a particular warm micro-climate (Fig. 7). In contrast, half of the locations show positive mean annual ground and ground surface temperatures (MAGT, MAGST). Hence, the SOs are generally positive and range from 0.5 to 7 °C. The TOs (thermal offsets or "temperature offsets in the near-surface" where the ground temperature is measured above the permafrost table) are often not significant and range from −2 to +1 °C.

The SOs are important for permafrost distribution and dominate the effects of TOs in these climatic conditions and surface types (mountain permafrost). In the following,

the results, and in particular the surface offsets, are presented and discussed regarding variations in surface characteristics, topography and macro-climate. However the variation in the parameters of interest (surface type, snow accumulation, slope, aspect, elevation, macro-climate etc.) is not systematic enough and the sample is too small (cf. Sect. 2.2) to quantify the offsets along all potential gradients. For example, specific air temperature and surface temperature lapse rates, which are important for permafrost distribution patterns in northern BC (Lewkowicz and Bonnaventure, 2011), can not be extracted from our data: a brief comparison of high and low elevation sites that lie in proximity simply indicates that pronounced winter inversions lead to small or non-existent laps rates of MATs between valley bottoms and hilltops (near tree line) what supports existing studies on this matter.

4.2 Surface and thermal offset by surface characteristics

First, we discuss the offsets of the mean annual temperatures regarding different surface characteristics. With surface characteristics we denote classes of near-surface ground properties (surface type), micro-topography and vegetation cover regarding their thermal influence. A brief information on that for all measurement locations was given in Table 1 in the columns surface type and note. These characteristics can vary within short distance and are responsible for a pronounced small-scale variability of ground temperatures; however, their influence may vary between sites with different macro-climatic conditions. In this section we quantify the effect of different surface characteristics on the surface and thermal offset (SO, TO) at our field sites. Even if the sample is too small and not systematic, as described above, we get a first estimate of the influence of surface characteristics on permafrost occurrence in British Columbia and compare them between sites.

Figure 8 shows the SO and TO of all locations ordered by surface characteristics based on a simple forehand classification: we distinguish on a first order between the classes rock, soil, debris, and forest. The class rock comprises near-vertical bedrock at different aspects and flat bare rock. Under soil we subsume fine-grained substrate

(mineral soils and colluvium) with minor vegetation such as alpine tundra (NON, PIN) or grassland (MID_wx). The class debris contains all surfaces with coarse debris covers that contain voids that allow air circulation. Finally, forest comprises different forest types such as black spruce, pine and alder forests. The substrate in these forests contains an organic soil layer with a moss cover where not otherwise marked (Fig. 8). A further meta information additionally to the surface classes is the exposure to solar radiation and wind (Fig. 8; top). These factors are influenced by the (micro-)topography and affect the snow deposition (wind) and the radiation balance (mainly insolation) when snow free.

The average SO per class does not show a clear dependency on the surface type. However, a comparison of the mean offsets may be misleading due to the bias by other influence factors (e.g. wind exposure). For average irradiation and wind conditions the SOs on flat bare rock (2.5–4 °C) appear to be slightly higher than for the other surface types, which are in the range of 1.5 to 3 °C Fig. 8). If not a bias of the snow cover influence, the difference compared to the SOs on soils (alpine tundra) may be explained by the lower albedo of the rock. Interestingly, the SOs on coarse debris are not significantly smaller than for the other surface types. Within the first 30–50 cm of the block layer no significant offset (see TO) was observed. Obviously the ventilation (Haeberli, 1973; Harris and Pedersen, 1998) and reduced thermal conductivity (Gruber and Hoelzle, 2008) of the block layer have no large effect on the thermal regime of our field sites.

Within the class near-vertical bedrock a variation in the SOs of 4 °C (SO: 1–5 °C) indicates the influence of aspect controlled irradiation on these snow free surfaces, which is discussed in more detail in the next section. Note that for this class no rock temperature at depth is measured, and that the near-surface temperature is used for the SO calculation. In the classes soil and debris, which comprise more gentle slopes with snow accumulation, the aspect control is smaller. The north–south difference of the SOs is about 2 °C for the alpine tundra at Nonda (NON_S vs. NON_N) and 1.5 to 3 °C in the coarse debris at Hudson Bay Mtn. (HUD_scr1–5 in Fig. 8). For coniferous

Characteristics of mountain permafrost in British Columbia

A. Hasler et al.

forests with a dense canopy (spruce, pine), where the SOs are approximately 2 °C, there is no difference between north and south slopes. However, the forest type, and correspondingly the canopy density, may be influenced by the aspect. This leads to significantly larger SOs where light forest and broadleaf trees allow higher incident solar radiation (e.g. POP_S in Fig. 8).

Wind exposed locations with only a thin snow cover lead to a smaller SO than at sheltered locations at all field sites. Whereas the SO at the three wind exposed locations in the rock mountains is 1 °C or less, the wind-swiped location at Huson Bay Mt. (HUD) has an SO of 2.7 °C (Fig. 8). This larger offset is possibly a result of more snow accumulation at wind exposed locations of HUD due to more frequent wet snowfall in the Coast Mountains: observed snow heights during site visits and measured surface temperature during winter indicate a more insulating snow cover at HUD_fl than at other locations, whereas wind gust measured at the meteo stations (wx) are similar at HUD and GUN and only slightly higher at NON and PIN. The local wind condition are not considered and can not be assessed with our data, hence a cross-checking of the above hypothesis is not possible at this point in time.

Regarding the influence of vegetation and organic layer on SO and TO, the field sites MID and POP are off special interest. At Middlefork the locations in open grassland (MID_wx), a palsa in a light stand of black spruce (MID_pf), and a pine forest with closed canopy on a gentle slope (MID_fr) indicate a decrease in SO with increasingly dense vegetation (Fig. 8). Hence the colder air temperature at the locations with lesser vegetation due to cold air drainage is overcompensated by these larger SOs (cf. Fig. 7). At the location with permafrost occurrence MID_pf, a clearly negative TO (–1.3 °C) is responsible for the permafrost occurrence (Fig. 8). If this TO is caused by a thermal diode effect of the moss layer or by a transient effect of the latent heat required to melt massive ice within the degrading palsa is not clear by this data alone. An additional cooling effect due to reduced snow height on the palsa usually described in the literature could not verified with our data because the smaller SO on the palsa compared to MID_wx is manly caused by summer temperatures (shading from black spruce or dif-

Characteristics of mountain permafrost in British Columbia

A. Hasler et al.

Title Page

Abstract	Introduction
Conclusions	References
Tables	Figures

◄ | ►

◄ | ►

Back | Close

Full Screen / Esc

Printer-friendly Version

Interactive Discussion

ferent depth of probe?). At the POP field site a clearly larger SO in contrast to the other locations is observed at POP_S (Fig. 8). This large SO is caused by warmer ground temperatures in summer. Hence, the higher transmissivity of the alder forest allows more irradiative warming of the ground compared to the spruce forest on the other locations. The three locations with a thick moss layer (POP_N1–3) show significant TOs between −0.8 and −1.7 °C. Similar to MID_pf the ground temperatures of these locations are at 0 °C throughout the year. Hence it is not clear here as well if these TOs reflect an equilibrium thermal diode effect or if they indicate degrading permafrost with high ice content.

4.3 Aspect control of rock temperatures on the example of near-vertical cliffs

Near-vertical rock temperatures are a good parameter to investigate the aspect control of ground temperatures and to validate downscaling and radiation algorithms in physically based permafrost models because no complex surface characteristics and snow cover complicate the situation. Gruber (2012) points out the importance of an extension of existing measurements to other environmental conditions for a better understanding of the drivers of these temperatures. In the first part of this section we describe the surface offsets in steep bedrock at the three high elevation sites GUN, PIN, and HUD and discuss them in comparison to near-vertical rock temperatures in other regions. After that we elaborate the thermal regime at Mt. Gunnel (GUN) with a numerical model simulation. An understanding of this specific situation is of particular interest because diverse rock slides emerged from similar topographic and geological situations in the northern BC (Geertsema et al., 2006).

The mean annual rock temperatures from the near-surface (MARST or MAGST) at Mt. Gunnel illustrate the aspect control of ground temperatures by solar irradiation. At the shaded north side (GUN_N) MAGST is just 0.9 °C higher than MAAT whereas this SO on the south side (GUN_S) is approximately 5 °C (Table 2). Subtracting these two north and south face SOs yields a difference of 4.1 °C. A significant east–west difference does not exist (cf. GUN_E and GUN_W, Table 2). The N–S difference at

Hudson Bay Mt. (HUD_S2 vs. HUD_N) is 3.8 °C. If not caused by differences in albedo or sky view factor, the slightly smaller N–S difference at HUD may be related to the higher cloudiness at Hudson Bay Mt. common in the more humid Coast Mountains. However, the difference is too small (not significant; cf. uncertainty in Fig. 8) to draw any conclusions on this macro-climatic effect. The effects was neither detectible in other empirical studies (Gruber, 2012). For Pink Mountain we cannot calculate the north–south difference because the corresponding aspects are not monitored. The SO values from PIN-SE and PIN-W correspond with similar aspects at GUN.

Compared with near-vertical rock temperatures in other mountain ranges, this influence of aspect, falls between the values of mid-latitude (Swiss and New Zealand Alps) and slightly higher latitude (Norway). In the Swiss Alps N–S differences from 6 to 8 °C are reported (Gruber et al., 2004; PERMOS, 2010; Hasler et al., 2011), in New Zealand this difference is about 6 °C (Allen et al., 2009), whereas in middle Norway differences of 3 to 3.5 °C where observed (Hipp et al., 2014). Strong (directional) reflection in the glacial environments of the Alps amplifies the short-wave incoming radiation on southern rock faces (Allen et al., 2009; Hasler et al., 2011) and makes the high values not directly comparable to the situation in this study. A stronger decay of the expositional difference of PISR occurs north of about 60° N (Gruber, 2012) where expositional differences in the range of 0.5 to 1.5 °C are reported at 80° N (Lewkowicz, 2001).

Within compact bedrock thermal offset effects are small and rock surface temperatures are a reasonable assumption to extrapolate (permafrost) temperature at depth. However, micro-topographic factors such as surface geometry and fractures in the rock influence the subsurface temperature field (Hasler et al., 2011). Figure 9 shows the situation at the GUN field site and the results of the heat conduction model (cf. Sect. 3.3) for this complex topography. It illustrates the cooling effect of fractured blocks due to cold (shadowy) surfaces in the cleft approaching air temperature and the cooling of wind-swept surface with a thin snow cover (cf. Sect. 4.2). In case of Mt. Gunnel the MAGST of the shadowy rock faces and the top surface is slightly below 0 °C whereas the other free surfaces have annual means above 0 °C (Fig. 9b). The steady state run

(Fig. 9c) indicates positive rock temperatures for the southern block and slightly negative temperatures for the northern block with possible permafrost occurrence. The small extent of the considered geometry requires, however, the consideration of the active layer thickness (ALT) to estimate permafrost occurrence in this very case. Figure 9d shows such an estimate applying the measured annual temperature amplitudes and a water saturated porosity of 5 % in a transient model run (cf. Sect. 3.3). With the given geometry these latent heat effects are critical for the permafrost occurrence reducing the ALT. The grey and light-blue areas in Fig. 9d indicate a very small permafrost body within the considered blocks.

More generally we can summarize, that the thermal conditions at GUN are very close to the limit for permafrost to occur. The micro-topography is essential for permafrost estimates at Mt. Gunnel. Warm permafrost is only expected in the following settings: below steep north faces, in fractured rock, under blocky layers and under wind-swept surfaces. Compact rock in E–S–W aspects and surfaces with snow accumulation (center of plateaus, forest) are unlikely to contain permafrost. Hence, the rock fall that occurred at Mt. Gunnel and the near-by Vanessa slide (Geertsema and Cruden, 2009) are possibly related to such local permafrost occurrence.

4.4 The influence of continentality on snow cover-induced surface offsets

Total annual precipitation, annual air temperature amplitude (ATA) and average cloud-cover are highly correlated on the large scale and distinguish humid maritime and dry continental climates (cf. Sect. 2). Continentality can be defined as ATA for a given latitude, or as the difference in monthly means of air temperature from the coldest and warmest month divided by two ($(T_{july} - T_{jan})/2$) (in some studies just the difference $T_{july} - T_{jan}$ is used). These macro-climatic differences are thought to modify the effectiveness of the physical processes responsible for the surface offsets and cause, together with variations in MAAT alone, meridional gradients on the continental scale of the lower limit of mountain permafrost (cf. King, 1986; Harris, 1989) and the southern extent of lowland permafrost (Harris, 1986). Guodong and Dramis (1992) report differ-

ent dependencies of the lower limit of mountain permafrost on continentality found for different latitudes in China. However, these early studies did not clearly distinguish between effects of MAAT, precipitation, and continentality because spatial information on these variables was sparse. With recent advances regarding such spatial data sets (interpolations and reanalysis of meteorological data) the dependency of surface offsets from continentality and precipitation are major macro-climatic unknowns for empirical permafrost maps. A recent empirical study on the Alpine-wide permafrost distribution found no significant dependency of rock glacier lower limit on precipitation (Boeckli et al., 2012). Even though the precipitation (and continentality) gradients in the Alps are comparably small, this result contradicts the hypothesis that the lower limit of mountain permafrost (or ground temperature) depends on macro-climatic variables other than MAAT and radiation.

Because our measurements span large gradients in continentality (cf. Sect. 2.1), they provide an opportunity to directly evaluate the effect of continentality on SO with field measurements of similar characteristics and to estimate its role for the permafrost distribution in British Columbia. In Sect. 4.3 we already stated that we could not demonstrate a significant effect of macro-climatic cloudiness in the irradiation-induced aspect control of SOs in near-vertical bedrock. While this topographic situation is quite marginal in terms of spatial representativeness, terrain with significant snow accumulation is widespread and requires consideration.

With increasing continentality less (winter) precipitation and, on average, a thinner snow cover is expected. Even though snow can have diverse cooling and warming effects, one of its main impacts and the dominant warming effect is the thermal insulation of the ground from winter air temperature (Zhang, 2005). This affects the nival offset, that part of the SO which is caused by insulation of the snow cover (Smith and Riseborough, 2002) leading to smaller offsets with thinner snow cover for a given MAAT and ATA (or freezing index). The larger annual air temperature amplitude coinciding with smaller annual precipitation on a macro-climatic scale may have a reverse effect on the nival offset. To what degree do these two effects balance each other, or does

Characteristics of mountain permafrost in British Columbia

A. Hasler et al.

Title Page

Abstract | Introduction

Conclusions | References

Tables | Figures

◄ | ►

◄ | ►

Back | Close

Full Screen / Esc

Printer-friendly Version

Interactive Discussion

one process clearly dominate? These questions have rarely been addressed in the literature so far.

The data shows no clear difference between Coast Range and continental side of the Rocky Mountains in terms of SOs. Generally, the measured ATA and the precipitation sum (Wang et al., 2012) correlate negatively with each other, however, the high elevation site in the inner Rocky Mountains (NON) shows a comparably low precipitation sum but rather small ATA as well (Fig. 10). Because the mean surface offsets per site shown in Fig. 10 are biased by the surface characteristics (compare Sect. 4.2) the missing dependency on this aggregation level is not surprising. Even locations from the same surface class do not show a consistent dependency on either ATA, nor on the total annual precipitation (Fig. 10). Despite the limitations of such a general comparison between sites, the largest SOs being observed at the driest location is surprising and motivates closer scrutiny.

The thermal diode model (Sect. 3.4) simulates the seasonal heat transfer between atmosphere and ground by simple snow insulation and related surface or nival offsets. In a brief sensitivity analysis with a pairwise parameter (ATA and snow insulation) different models were compared, referred to as the exact model, the n factor model and the variable insulation model (cf. Sect. 3.4). Each model was run with two parameter sets ($A = 10\,^{\circ}\mathrm{C}$ and $R_\mathrm{s} = 20$; $A = 20\,^{\circ}\mathrm{C}$ and $R_\mathrm{s} = 10$). In Fig. 11 the results of four of these model runs over 8 years (2900 days) are presented. All simulations show consistently that the SO is larger with doubled amplitude and half of the snow insulation value (cf. Fig. 11b and c). This is simply explained in the example of the n factor model. The integral of the negative temperatures (freezing index If: gray area in Fig. 11) is larger for the larger ATA under the same MAAT. Hence, the amplitude effect over-compensates the snow insulation effect for given settings. This will vary slightly for different surface types and ground thermal characteristics (change in R_gr), and the thermal properties of the snow cover for real world situations. Nonetheless, the strong compensation effect of the ATA remains unchanged because the difference between winter and summer air temperature is the primary driver of the nival offset where significant snow cover

built-up takes place. This is consistent with the finding of Goodrich (1982), that ATA has a on the snow cover effect. This influence is implicitly considered in distributed n factor models such as e.g. TTOP (Smith and Riseborough, 2002), which are mainly applied for low-land permafrost. For mountain permafrost, where empirical models apply topographical parameterizations of the SO, the influence of the ATA has not been investigated so far.

The nival offset considers only the insulation effect during freezing days – a clear limitation for cold humid climates where snow cover persists for a significant part of the early summer (Zhang, 2005). To further investigate the nival offset and other effects of the snow cover on the surface offset two locations were compared from the dataset. While these sites have the largest difference in terms of macro-climate, both accumulate snow without much influence of wind. The site HUD_fl is a near-horizontal rock surface on the south slope of Hudson Bay Mtn. with a thick winter snow cover. In contrast, MID_wx is located on a grassy gentle sloping till (fine-grained soil) next to a river, with no particular shading or wind influence as well, but in a much drier and more continental climate (cf. Table 1). The MAAT at both locations is around $-3\,°C$ and the influence of differences in moisture content (soil vs. bedrock) is apparently not affecting the surface temperature measurements (no significant zero curtain at the soil site). These two locations are compared in Fig. 12. The ground surface and air temperature (Fig. 12 top) are subtracted to show the seasonal contribution to the SO (Fig. 12 middle). This shows clearly that the nival offset (orange area during winter) is larger in the case of MID_wx even though the ground surface is colder at this location during winter. The seasonal and biweekly freezing N factors (Fig. 12 bottom N_{fr}) are smaller at MID_wx, indicating a less insulating snow cover. Hence, in this example, the effect of the ATA overwhelms the effect of the snow cover thickness on the nival offset similar to the model study above. However, a striking difference between the temperature regimes at the two locations is the difference in thawing N factor (Fig. 12 bottom N_{th}). At MID_wx, where the entire summer is snow free, N_{th} is close to one, whereas at HUD_fl the snow cover persists until August and leads to a strong reduction of N_{th} by albedo

Characteristics of mountain permafrost in British Columbia

A. Hasler et al.

and latent heat effects. The resulting negative summer offset at HUD (Fig. 12 middle; blue area) further reduces the SO. In this comparison the maritime humid climate leads to an SO of 3.9 °C due to a smaller temperature amplitude and a long-lasting snow cover while the drier continental climate results in a SO of 6.1 °C.

⁵ These numbers may not easily be generalized because local wind conditions will strongly modify the persistence of the snow cover at other locations, but the influence of the ATA will remain important everywhere that an insulating snow cover (> 0.4 m) builds up. This is supported by a study from Throop et al. (2012) that analyses measurements from throughout northern Canada, showing similar SOs at sites near the Coast Range ¹⁰ (Wolf Creek Sites, Yukon) and west of the Hudson Bay (Baker Lake Site, Nunavut) with strong differences in annual temperature amplitude and precipitation: even though the N_{fr} differ strongly between these sites (0.4 vs. 0.7), all SOs are around 3.2 °C (cf. Throop et al., 2012 Tables 1 and 2). For all considered sites in this study, the SO shows a minor dependency on MAAT but the N_{fr} is systematically larger with more negative ¹⁵ MAAT (Throop et al., 2012). This is explained not only by the delayed freeze back of the thick active layer in warm ice-rich permafrost (Smith and Riseborough, 2002), but also by generally larger ground freezing indexes in cold permafrost due to the lower ground temperatures (relevant if ice content is low).

The outcome of this analysis is the hypothesis, that the macro-climatic effect on ²⁰ snow-cover induced SOs is much smaller than expected from local studies, where only the snow-cover thickness varies but similar air temperature amplitudes force the heat fluxes. In humid to semi-dry conditions where a significant snow cover builds-up takes place, the corresponding differences in the ATA strongly compensate for the effects of snow cover insulation (Fig. 13). This is an important outcome for the application of ²⁵ empirical mountain permafrost models, which apply topographical parameterizations of the surface offset, over large areas with significant macro-climatic variations. A further consequence from the dependency shown in Fig. 13 is the strong sensitivity on snow cover change for continental climates due to the large ATA.

5 Conclusion

This study comprises the pre-processing and analysis of an extensive but heterogeneous data set of ground temperatures that is novel for the province of British Columbia. Regarding the treatment of similar data a methodical outcome is:

Data processing

– The used calculation of mean annual temperatures and its uncertainty analysis allows a comparison of inconsistent data for a "quasi-static" surface offset-/thermal offset-analysis.

The main focus of the paper is the quantification and description of the surface offset and thermal offsets regarding the three influencing factors surface characteristics, topography and macro-climate. The respective key findings are listed separately as follows:

Surface characteristics

– The average of the surface offsets per class of surface type (rock, fine soil, coarse debris, forest) is 2 to 2.5 °C with no clear difference between classes.

– Wind-swept surfaces have a smaller surface offset (below 1 °C). In one case the offset is larger, possibly due to more frequent wet snowfall.

– Thermal offsets are negligible, except at north facing forest sites with a thick organic layer (moss) where they are −1 to −2 °C. It is not clear if these thermal offsets represent equilibrium conditions because the temperature at the permafrost table is constantly at 0 °C and transient effects may be important under such conditions. This study only included one wetland (with peat) due to its focus in mountain permafrost.

– Surprisingly the surface offset on coarse blocky material is not smaller and no thermal offsets are detected in the upper most layers (0.3–0.5 m).

Aspect control of insolation and other topographic effects

- The north–south difference of the surface offset in near-vertical bedrock is 4 °C. No east–west difference was detected.

- On gentle slopes (angle < 30°) on alpine tundra or debris the observed north–south difference is between 1.5 and 3 °C. In forests with a dense canopy this difference is negligible.

- A detailed modelling study for the Mt. Gunnel site shows that the cuesta (gently sloping table-top mountain) is very close to the limit of permafrost. The cooling effect of clefts in the bedrock is important for permafrost occurrence at this site.

Macro-climate

- The aspect control of the surface offset in steep bedrock does not show significant differences between different macro-climatic regions.

- The effect of snow cover insulation (nival offset) in the humid Coast Mountains and the semi-dry occidental side of the Rocky Mountains is similar. This is due to the reverse effect of the continentality (annual air temperature amplitude) which compensates for the decreased insulation (smaller freezing N factor) with lower winter temperatures (larger freezing index) in the continental climate.

- At snow-rich sites the long-lasting snow cover further reduces the surface offset by albedo and latent heat effects during early summer.

Regarding future estimates of permafrost distribution in British Columbia, local variability of the surface offset caused by topographic gradients is most important. This variability differs with vegetation and organic soil layers (which also controls the thermal offset) but is influenced only to minor extent by the macro-climatic variations.

The Supplement related to this article is available online at doi:10.5194/tcd-8-4779-2014-supplement.

References

Allen, S. K., Gruber, S., and Owens, I. F.: Exploring steep bedrock permafrost and its relationship with recent slope failures in the Southern Alps of New Zealand, Permafrost Periglac., 20, 345–356, 2009.

Boeckli, L., Brenning, A., Gruber, S., and Noetzli, J.: A statistical approach to modelling permafrost distribution in the European Alps or similar mountain ranges, The Cryosphere, 6, 125–140, doi:10.5194/tc-6-125-2012, 2012.

Bonnaventure, P. P., Lewkowicz, A. G., Kremer, M., and Sawada, M. C.: A permafrost probability model for the southern Yukon and northern British Columbia, Canada, Permafrost Periglac., 23, 52–68, 2012.

Cermak, V. and Rybach, L.: Thermal conductivity and specific heat of minerals and rocks, Landolt-Bornstein, Zahlenwerte and Funktionen aus Naturwissenschaften and Technik, 305–343, 1982.

Egginton, V. N.: Historical climate variability from the instrumental record in northern British Columbia and its influence on slope stability, Department of Earth Sciences – Simon Fraser University, 2005.

Fiddes, J. and Gruber, S.: TopoSCALE v.1.0: downscaling gridded climate data in complex terrain, Geosci. Model Dev., 7, 387–405, doi:10.5194/gmd-7-387-2014, 2014.

Geertsema, M. and Cruden, D. M.: Rock movements in northeastern British Columbia, in: Landslide Processes: From Geomorphologic Mapping to Dynamic Modelling, Proceedings of the Landslide Processes Conference: a tribute to Theo van Asch, edited by: Malet, J. P., Remaitre, A., Bogaard, T., Strasbourg, 6–7 February, CERG, Strasbourg, France, 31–36, 2009.

Geertsema, M., Clague, J. J., Schwab, J. W., and Evans, S. G.: An overview of recent large catastrophic landslides in northern British Columbia, Canada, Eng. Geol., 83, 120–143, 2006.

Goodrich, L. E.: The influence of snow cover on the ground thermal regime, Can. Geotech. J., 19, 421–432, 1982.

Gruber, S.: A Global view on permafrost in steep bedrock, in: Proceedings of the 10th International Conference on Permafrost, Salekhard, Russia, 25–29 June 2012, 131–136, 2012

Gruber, S. and Hoelzle, M.: The cooling effect of coarse blocks revisited: a Modeling Study of a Purely Conductive Mechanism, in: Proceedings of the Ninth International Conference on Permafrost, Fairbanks, Alaska, USA, 29 June–3 July 2008, 557–561, 2008.

Characteristics of mountain permafrost in British Columbia

A. Hasler et al.

Title Page

Abstract	Introduction
Conclusions	References
Tables	Figures

Back | Close

Full Screen / Esc

Printer-friendly Version

Interactive Discussion

Gruber, S., Hoelzle, M., and Haeberli, W.: Rock-wall temperatures in the Alps: modelling their topographic distribution and regional differences, Permafrost Periglac., 15, 299–307, 2004.

Gubler, S., Fiddes, J., Keller, M., and Gruber, S.: Scale-dependent measurement and analysis of ground surface temperature variability in alpine terrain, The Cryosphere, 5, 431–443, doi:10.5194/tc-5-431-2011, 2011.

Guodong, C. and Dramis, F.: Distribution of mountain permafrost and climate, Permafrost Periglac., 3, 83–91, 1992.

Haeberli, W.: Die Basis-Temperatur der winterlichen Schneedecke als möglicher Indikator für die Verbreitung von Permafrost in den Alpen, Zeitschrift für Gletscherkunde und Glazialgeologie, 9, 221–227, 1973.

Harris, C., Arenson, L. U., Christiansen, H. H., Etzelmüller, B., Frauenfelder, R., Gruber, S., Haeberli, W., Hauck, C., Hölzle, M., and Humlum, O.: Permafrost and climate in Europe: Monitoring and modelling thermal, geomorphological and geotechnical responses, Earth-Sci. Rev., 92, 117–171, 2009.

Harris, S. A.: Permafrost distribution, zonation and stability along the eastern ranges of the cordillera of North America, Arctic, 39, 29–38, 1986.

Harris, S. A.: Continentality Index: Its uses and limitations applied to permafrost in the Canadian Cordillera, Physi. Geogr., 10, 270–284, 1989.

Harris, S. A.: Climatic change and permafrost stability in the eastern Canadian Cordillera, in: Extended Abstracts of the Ninth International Conference on Permafrost, Fairbanks, Alaska, USA, 29 June–3 July 2008, 93–94, 2008

Harris, S. A. and Pedersen, D. E.: Thermal regimes beneath coarse blocky materials, Permafrost Periglac., 9, 107–120, 1998.

Hasler, A., Gruber, S., and Haeberli, W.: Temperature variability and offset in steep alpine rock and ice faces, The Cryosphere, 5, 977–988, doi:10.5194/tc-5-977-2011, 2011.

Hipp, T., Etzelmüller, B., and Westermann, S.: Permafrost in alpine rock faces from Jotunheimen and Hurrungane, Southern Norway, Permafrost Periglac., 25, 1–13, 2014.

Karunaratne, K. C. and Burn, C. R.: Freezing n factors in discontinuous permafrost terrain, Takhini River, Yukon Territory, Canada, in: Proceedings of the 8th International Conference on Permafrost, Zurich, University of Zurich-Irchel. S., 519–524, 2003.

King, L.: Zonation and ecology of high mountain permafrost in Scandinavia, Geogr. Ann. A, 131–139, 1986.

Characteristics of mountain permafrost in British Columbia

A. Hasler et al.

Title Page

Abstract | Introduction

Conclusions | References

Tables | Figures

|◀ | ▶|

◀ | ▶

Back | Close

Full Screen / Esc

Printer-friendly Version

Interactive Discussion

Lewkowicz, A. G.: Temperature regime of a small sandstone tor, latitude 80° N, Ellesmere Island, Nunavut, Canada, Permafrost Periglac., 12, 351–366, 2001.

Lewkowicz, A. G. and Bonnaventure, P. P.: Equivalent elevation: a new method to incorporate variable surface lapse rates into mountain permafrost modelling, Permafrost Periglac., 22, 153–162, 2011.

Lunardini, V.: Theory of n factors and correlation of data, in: Proceedings of the Third International Conference on Permafrost, Edmonton, Alberta, Canada, 10–13 July 1978, 40–46, 1978

Mottaghy, D. and Rath, V.: Latent heat effects in subsurface heat transport modelling and their impact on palaeotemperature reconstructions, Geophys. J. Int., 164, 236–245, 2006.

Nakamura, R. and Mahrt, L.: Air temperature measurement errors in naturally ventilated radiation shields, J. Atmos. Ocean. Tech., 22, 1046–1058, 2005.

Noetzli, J.: Modeling transient three-dimensional temperature fields in mountain permafrost, Zurich, Switzerland: University of Zurich, 2008.

Noetzli, J. and Gruber, S.: Transient thermal effects in Alpine permafrost, The Cryosphere, 3, 85–99, doi:10.5194/tc-3-85-2009, 2009.

PERMOS: Permafrost in Switzerland 2006/2007 and 2007/2008, Glaciological Report (Permafrost) No. 8/9, edited by: Noetzli, J. and Vonder Muehll, D., Cryospheric Commission of the Swiss Academy of Sciences, Zurich, Switzerland, 2010.

Riseborough, D., Shiklomanov, N., Etzelmuller, B., Gruber, S., and Marchenko, S.: Recent advances in permafrost modelling, Permafrost Periglac., 19, 137–156, 2008.

Schneider, S., Hoelzle, M., and Hauck, C.: Influence of surface and subsurface heterogeneity on observed borehole temperatures at a mountain permafrost site in the Upper Engadine, Swiss Alps, The Cryosphere, 6, 517–531, doi:10.5194/tc-6-517-2012, 2012.

Smith, M. W. and Riseborough, D. W.: Climate and the limits of permafrost: a zonal analysis, Permafrost Periglac., 13, 1–15, 2002.

Throop, J., Lewkowicz, A. G., Smith, S. L., and Burn, C. R.: Climate and ground temperature relations at sites across the continuous and discontinuous permafrost zones, northern Canada, Can. J. Earth Sci., 49, 865–876, 2012.

Wang, T., Hamann, A., Spittlehouse, D. L., and Murdock, T. Q.: ClimateWNA-High-resolution spatial climate data for western North America, J. Appl. Meteorol. Clim., 51, 16–29, 2012.

Zhang, T.: Influence of the seasonal snow cover on the ground thermal regime: an overview, Rev. Geophys., 43, RG4002, doi:10.1029/2004RG000157, 2005.

Title Page

Abstract | Introduction

Conclusions | References

Tables | Figures

|◄ | ►|

◄ | ►

Back | Close

Full Screen / Esc

Printer-friendly Version

Interactive Discussion

Table 1. Measurement locations at all field sites. Locations with common parameters are summarized.

Site	Location[*]	Elevation (m a.s.l.)	Slope (°)	Aspect (°)	Surface Type	Note
GUN	wx	1470	0	–		no ground T
GUN	cr	1470	90	240	rock cleft	no snow
GUN	N, E, S, W	1470	90	0, 95, 195, 270	rock	no snow
GUN	SW, NW	1470	90	245, 330	rock	no snow
GUN	fl	1470	0	–	thin soil on rock	wind exposed
HUD	wx	1670	10	10, 220		no ground T
HUD	S2, S3, NW, N, NE	1970 (S)/2140	50–90	180, 240, 285, 350, 60	rock	no snow
HUD	fl, cx	2020	0–10	–, 40	rock	different snow
HUD	scr1–5	2030–2160	0–30	190, 190, –, –, 0	coarse debris	snow covered
MID	wx	1000	0	–	soil, grass	cold air drainage
MID	pf	1010	0	–	soil and moss	palsa, black spr.
MID	fr	1020	10	210	soil and moss	aspen forest
NON	wx	1680	0	–	alpine tundra	wind exposed
NON	N, S	1670	15–20	0, 180	alpine tundra	wind exposed
PIN	wx	1750	0	–		no ground T
PIN	W, SE	1740	90	285, 135	rock	no snow
PIN	cx, cc	1750	0	–	alpine tundra	different snow
PIN	ls	1740	25	80	coarse debris	snow covered
POP	N1 – N3	780–940	15–30	0, 0, 10	soil and moss	black spruce f.
POP	N4[**], S	940, 750	30, 15	10, 180	soil, light forest	[**]on landslide
POP	SW	890	35	240	fine grain. debris	colluvium
TET	S1, S2	1010	25	170	soil and moss	aspen-pine f.
TET	N1, N2	1010	25	10	soil and moss	black spruce f.

[*] location labeles: wx = weather station, cr = crack, N, E, S, W etc. = aspect, fl = flat, cx = convex, cc = concave, scr = scree, pf = permafrost, fr = forest, ls = landslide

Table 2. Surface offsets for all monitored near-vertical cliffs.

Site-location	Aspect (°)	Surface offset (°C)
GUN-N	0	0.9
GUN-E	95	2.5
GUN-S	195	5
GUN-SW	245	4
GUN-W	270	2.2
GUN-NW	330	1.1
HUD-S2	180	4.8
HUD-NW	285	1
HUD-N	350	1
PIN-SE	135	4.1
PIN-W	285	1.4
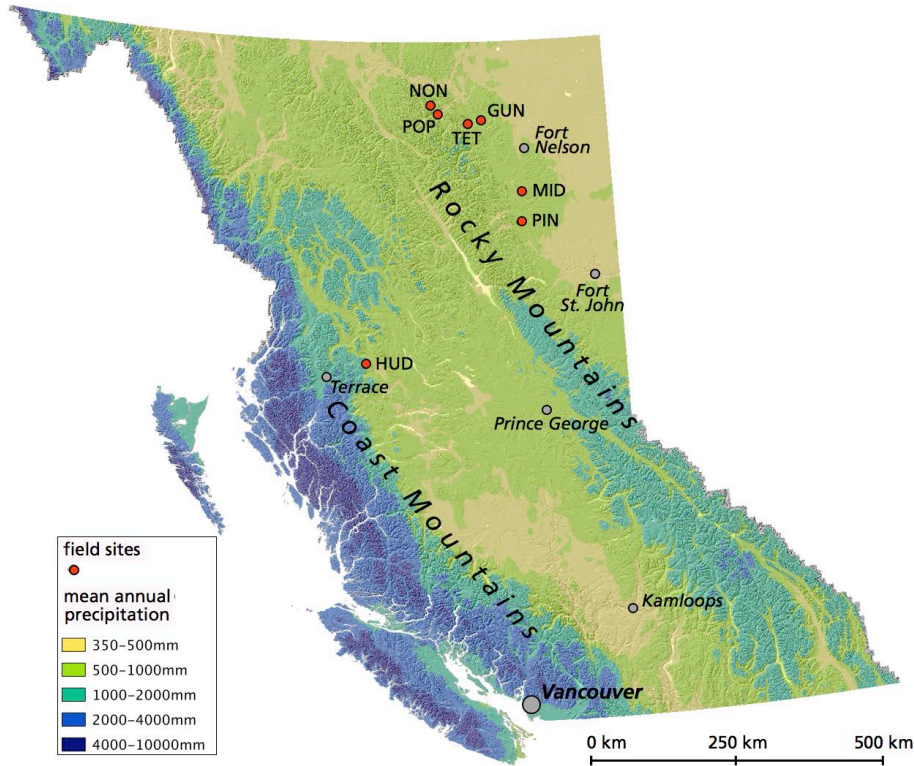
Figure 1. Overview of the field sites on a precipitation map of British Columbia. The field sites span a latitudenal range from 54°45′ to 59° N and are located within or close to the Coast Mountains and Rocky Mountains. These two main mountain ranges cause large gradients in precipitation and continentality within short distance (precipitation data from Wang et al., 2012).
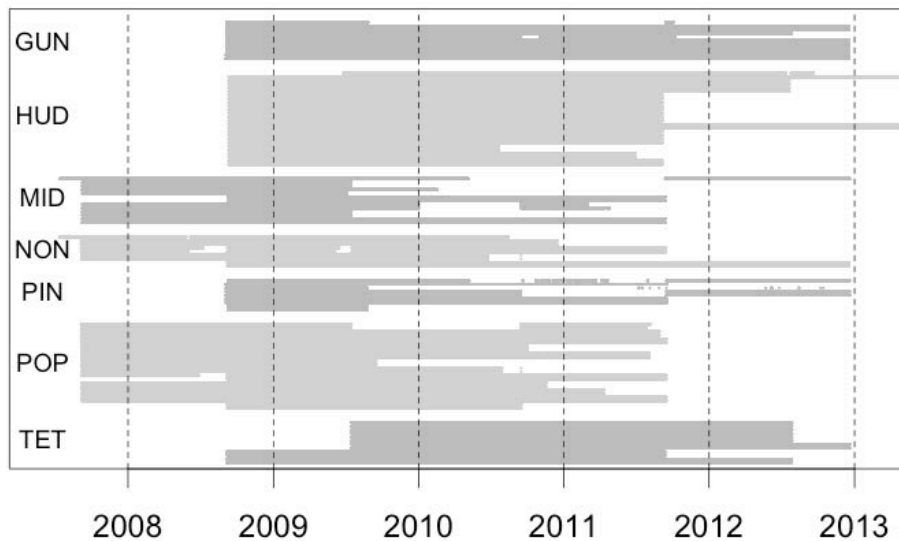
Figure 2. Data compleetness for the seven field sites. Grey bars indicate the presence of valid data.

Title Page

Abstract | Introduction

Conclusions | References

Tables | Figures

|◀ | ▶|

◀ | ▶

Back | Close

Full Screen / Esc

Printer-friendly Version

Interactive Discussion
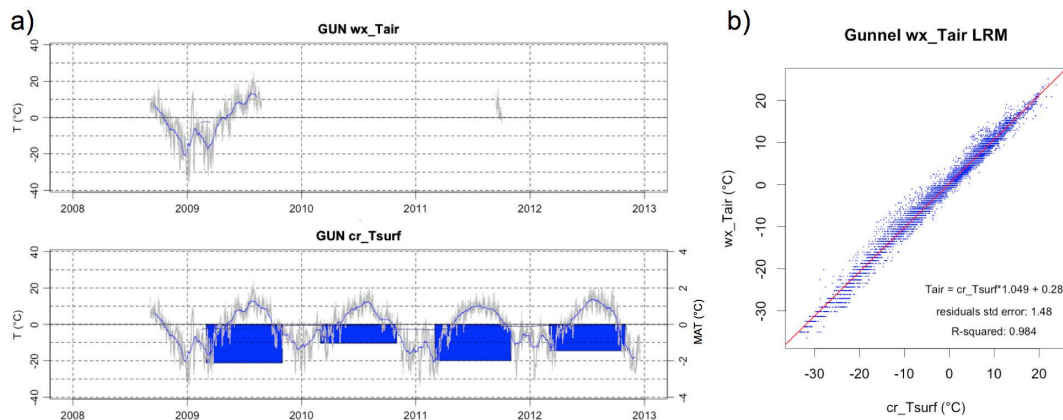
Figure 3. (a) Time series of weather station air temperature and surface temperature in rock cleft (grey = raw and blue line = running monthly means) at Mt. Gunnel. Blue bars are mean annual temperatures (MAT) on right scale. **(b)** Linear regression model for wx_Tair with scatter data (blue dots) and regression function (red line).
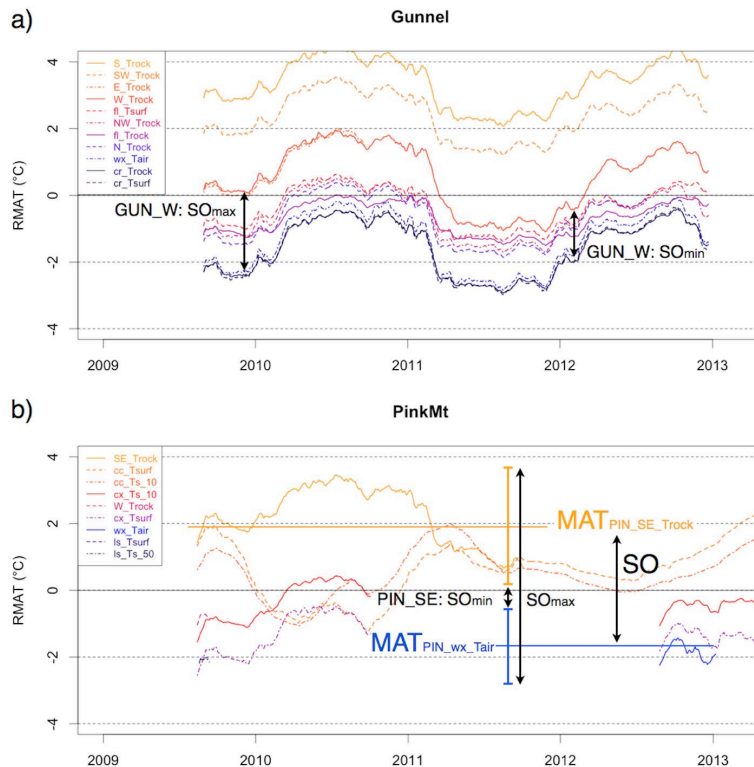
Figure 4. Two examples of running mean annual temperatures (RMAT). **(a)** Mt. Gunnel. Mainly near-surface rock temperatures from steep rock faces without snow. All temperatures have similar variations in annual means. **(b)** Pink Mountain. The annual means from convex and concave landforms show inverse development. Offset terms strongly depend on the point in time of the comparison of instantaneous MATs. These two examples are the best and worst case in terms of data completeness (compare Fig. 2). Indications of maximum and minimum surface offset are explained in text.

Full Screen / Esc

Printer-friendly Version

Interactive Discussion
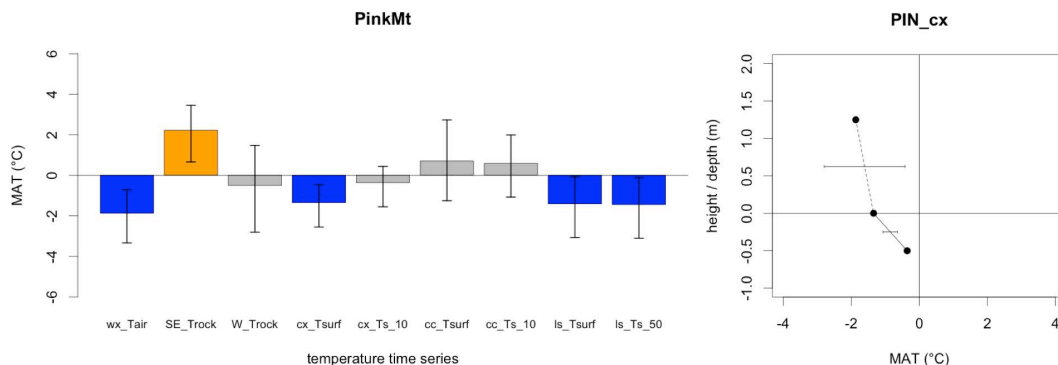
Figure 5. Examples from Pink Mountain of variation in MAT and uncertainties in offsets. Left: mean annual temperatures and spread for general intercomparison, orange bars are RMAT values above zero of enire measurement period, blue bars are entirely sub-zero RMATs; right: MAT profile with spread ($U_{offset}/2$) of the surface/thermal offsets. Solid lines indicate offsets that are larger than the spreads, dashed lines are used if offset is equal or smaller than the spread. The temperature at 1.4 m height is the mean annual air temperature (MAAT).
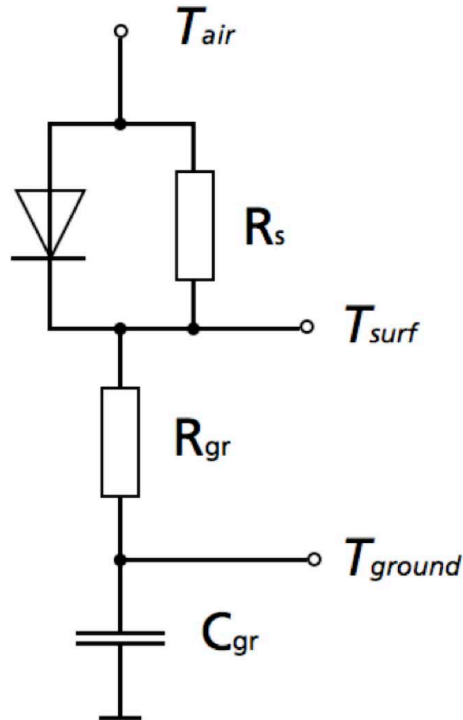
Figure 6. Thermal diode model: if air temperature T_{air} is bigger than T_{surf} the heat is transferred efficiently (diode) to the surface. During winter the snow cover acts as an insulator (resistor R_s) from air temperature. The ground temperatures T_{ground} are the dampened signal from the surface with the ground acting as an R-C element with R_{gr} being a heat-resistor (inverse thermal conductivity) and C_{gr} simulating the ground heat capacity (here we neglect thermal diode effects in the ground because we focus on the surface offset).

Full Screen / Esc

Printer-friendly Version

Interactive Discussion

Figure 7. Overview of all thermal profiles measured at 44 locations within the seven field sites. The temperatures at 1.4 m height are the mean annual air temperatures (MAAT). Dashed lines indicate offsets below the inward uncertainty (Offset $< U_{offset}/2$) of these offsets (Sect. 3.2). Solid lines indicate significant offsets.
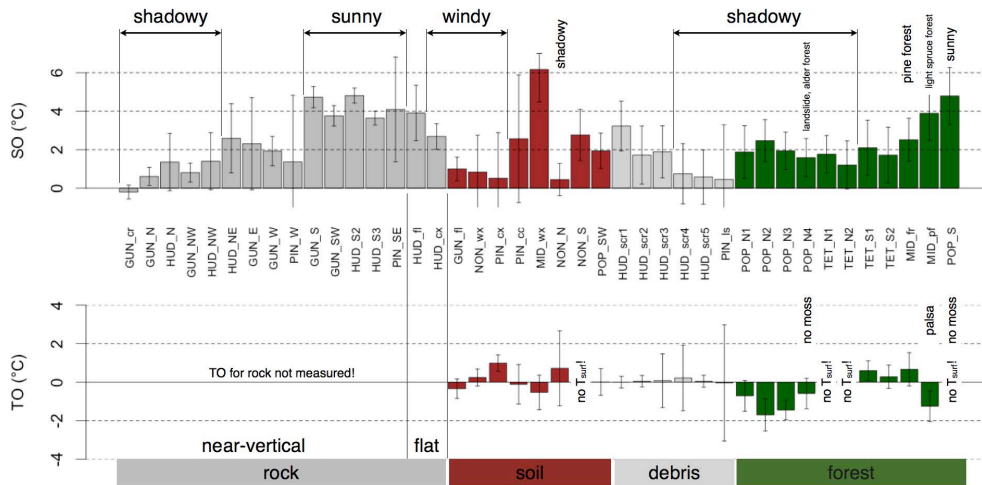
Figure 8. Surface and thermal offsets grouped by different surface types (substrate and vegetation) and with indication of micro-topographic situation and forest type.
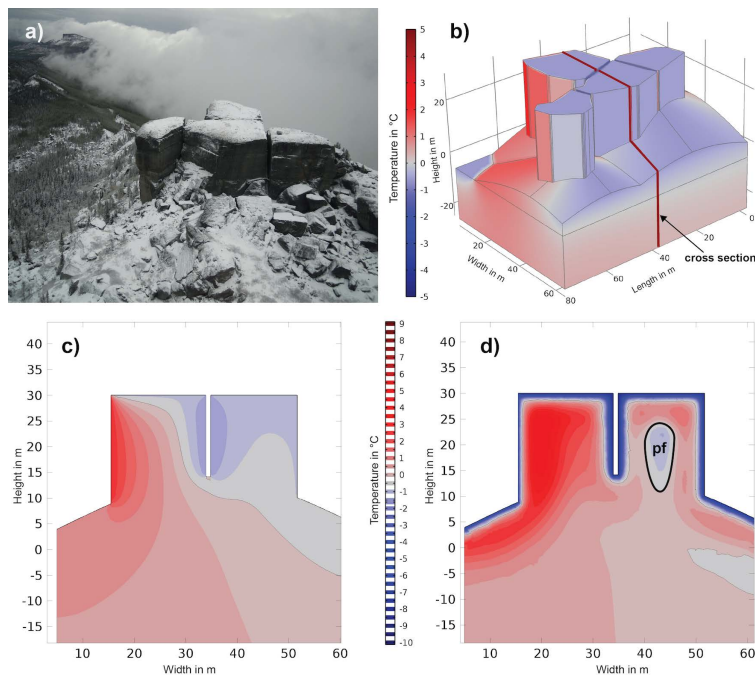
Figure 9. Sketched model of the Gunnel blocks and simulation results. **(a)** View on the Gunnel blocks from the North (Photo M. Geertsema). **(b)** Geometry of the model and colored surfaces according to mean annual ground temperatures (MAGST). The red line indicates the position of the North–South slice shown in **(c)** and **(d)**. **(c)** Mean subsurface temperatures (MAGT) in the Gunnel blocks shown for a vertical cross-section and a steady state simulation. The 0 °C isotherm is visualized by a black line. **(d)** Transient simulation of subsurface temperatures at the time of maximum thaw depth end of November. In **(d)** pf indicates local permafrost occurrence.

Full Screen / Esc

Printer-friendly Version
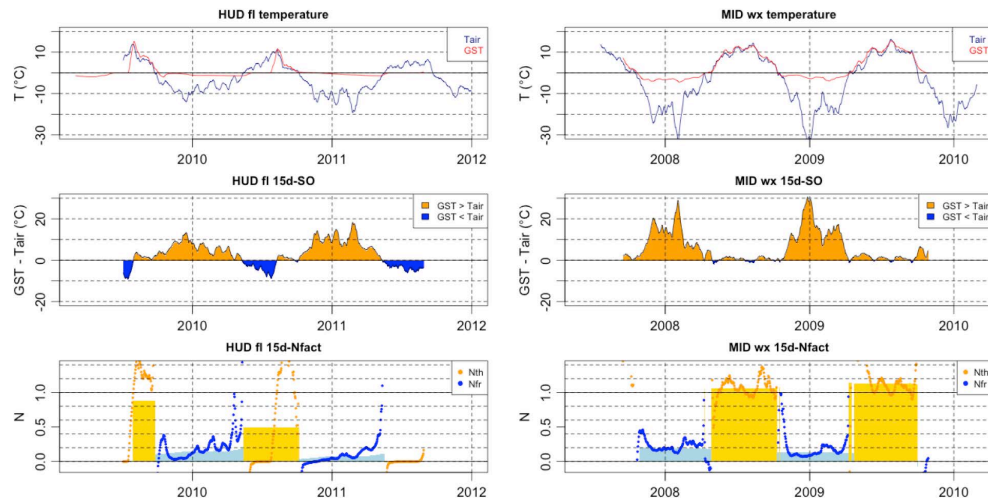
Interactive Discussion
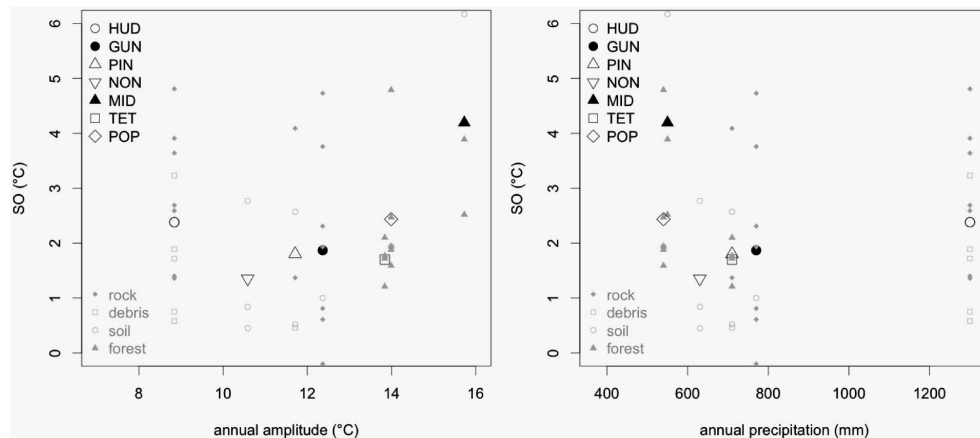
Figure 10. Surface offsets (SO) against macro-climatic parameters. Large symbols are means per site and small symbols are individual locations with symbol given by surface type. Left: SO against measured annual amplitude of air temperature (ATA = $(T_{july} - T_{jan})/2$); right: SO against annual precipitation sum (precipitation estimate from Wang et al., 2012).
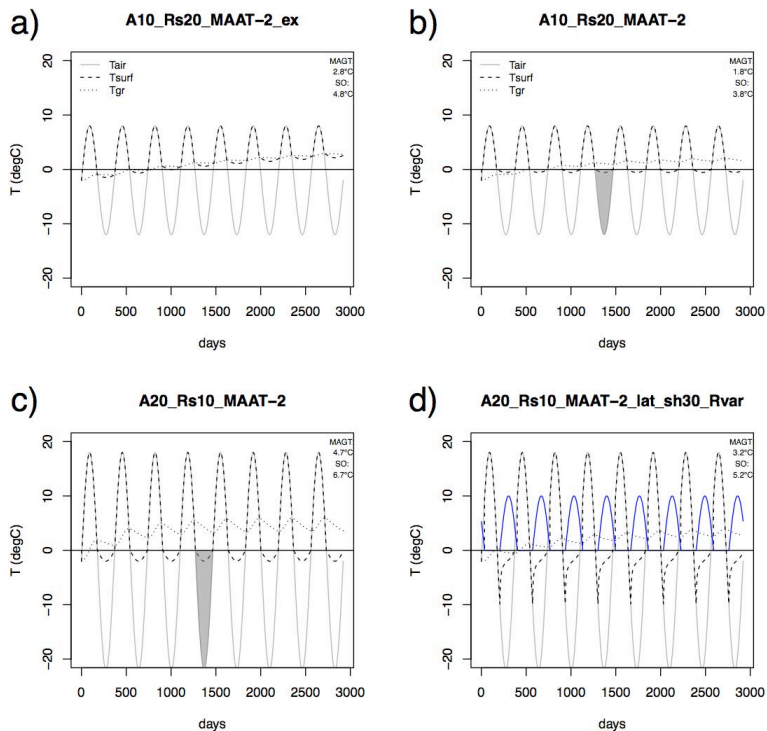
Figure 11. Four simulation results from the thermal diode model. **(a)** Exact model according to the diode scheme (Fig. 6) with an air temperature amplitude (*A*) of 10 °C and a snow cover resistivity (Rs) of 20 and MAAT = −2 °C; **(b)** model with diode triggering if air temperature is at 0 °C (similar effect as *n* factor) with same *A* and Rs; **(c)** same model with double amplitude (*A* = 20 °C) and half resistivity (Rs = 10); **(d)** model including variable Rs (blue line), shift of insulation effect (30 days) and snow latent heat effect with *A* = 20 °C and Rs_peak = 10. MAGT is calculated for the last of the 8 annual cycles, which is at to the long-term stabilization. Grey area corresponds to the freezing index (If).

Title Page

Abstract | Introduction

Conclusions | References

Tables | Figures

|◄ | ►|

◄ | ►

Back | Close

Full Screen / Esc

Printer-friendly Version

Interactive Discussion

Full Screen / Esc

Figure 12. Seasonal development of temperature differences and *N* factors at HUD_fl (left) and MID_wx (right). Top: raw temperatures; middle: temperature difference ($T_{surf} - T_{air}$) on 15 days running average; bottom: *N* factors on seasonal average (areas) and 15 days average (points). The SO is to one part controlled by the winter air temperature and is larger at MID_wx (orange area middle). Freezing *N* factors (N_{fr}) are on a similar level (0.1–0.2), whereas thawing *N* factors (N_{th}) differ due to the persistence of the snow during summer at HUD_fl.
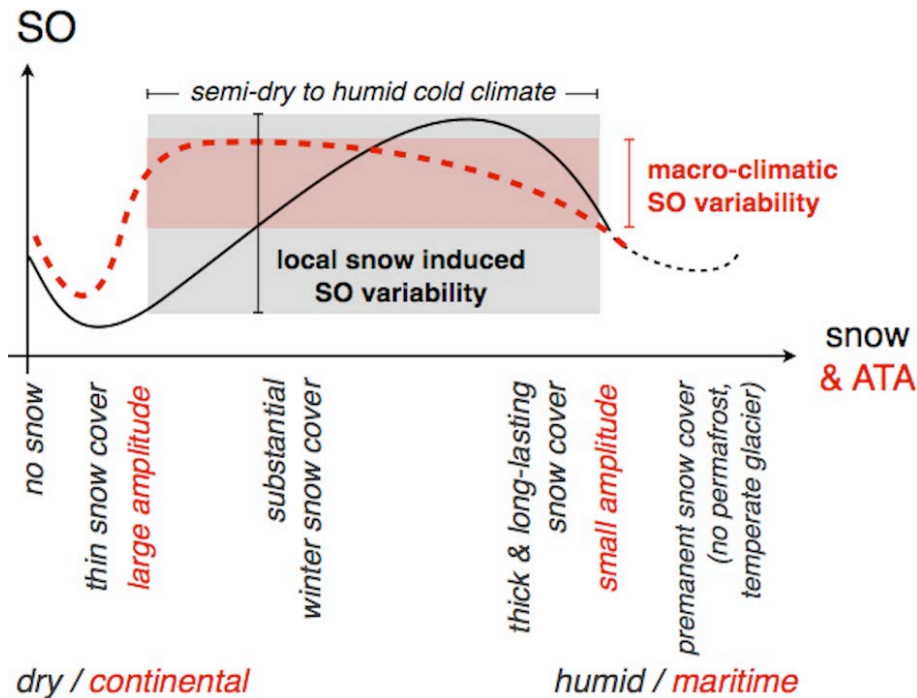
Figure 13. Qualitative sketch of the effect of snow cover thickness and air temperature amplitude (ATA) on the surface offset (SO): the dashed red line indicates the dependency on a macro-climatic continentality gradient (ATA) correlated with an increase in precipitation (and snow thickness; strong seasonality of precipitation is neglected). The black line corresponds to the effect of local variations in snow accumulation (wind drift etc.) but constant ATA. While SO increases with snow thickness for local variations until the effect of snow persistence reverses the trend, the continentality effect leads to a small variation of the SO for semi-dry to humid conditions. A possible warming effect of persistent snow cover due to water percolation (Zhang, 2005) may led to another increase of SO at the right-hand side.